Upscaling, integration and electrical characterization of molecular junctions

PAUL A. VAN HAL[1], EDSGER C. P. SMITS[1,2,3], TOM C. T. GEUNS[1], HYLKE B. AKKERMAN[2], BIANCA C. DE BRITO[1], STEFANO PERISSINOTTO[4], GUGLIELMO LANZANI[4], AUKE J. KRONEMEIJER[2], VICTOR GESKIN[5], JÉRÔME CORNIL[5], PAUL W. M. BLOM[2], BERT DE BOER[2] AND DAGO M. DE LEEUW[1,2]*

[1]Philips Research Laboratories, High Tech Campus 4, 5656 AE Eindhoven, Netherlands
[2]Molecular Electronics, Zernike Institute for Advanced Materials, University of Groningen, Nijenborgh 4, 9747 AG Groningen, Netherlands
[3]Dutch Polymer Institute, PO Box 902, 5600 AX Eindhoven, Netherlands
[4]IIT Istituto Italiano di Tecnologia, Dipartimento di Fisica, Politecnico di Milano, P.za L. da Vinci 32, 20133, Milano, Italy
[5]Service de Chimie des Materiaux Nouveaux, Université de Mons-Hainaut, Place du Parc 20, Mons, Belgium
*e-mail: dago.de.leeuw@philips.com

Published online: 19 October 2008; doi:10.1038/nnano.2008.305

The ultimate target of molecular electronics is to combine different types of functional molecules into integrated circuits, preferably through an autonomous self-assembly process. Charge transport through self-assembled monolayers has been investigated previously, but problems remain with reliability, stability and yield, preventing further progress in the integration of discrete molecular junctions. Here we present a technology to simultaneously fabricate over 20,000 molecular junctions—each consisting of a gold bottom electrode, a self-assembled alkanethiol monolayer, a conducting polymer layer and a gold top electrode—on a single 150-mm wafer. Their integration is demonstrated in strings where up to 200 junctions are connected in series with a yield of unity. The statistical analysis on these molecular junctions, for which the processing parameters were varied and the influence on the junction resistance was measured, allows for the tentative interpretation that the perpendicular electrical transport through these monolayer junctions is factorized.

Molecular electronics is the study of charge transport through single molecules or through a monolayer of molecules. The transport has been measured with a variety of techniques such as mechanically controlled break junctions (MCBJ) and conducting atomic force microscopy (C-AFM)[1–6]. The current–voltage characteristics have shown useful phenomena such as bistability and rectification. The combination of such functional molecules into integrated circuits of discrete junctions is a major goal in molecular electronics.

The most studied systems in molecular electronics are self-assembled monolayers (SAMs) of alkane(di)thiols on gold[7–9]. The resistance of gold/SAM/gold junctions is independent of temperature and exponentially dependent on the length of the molecule. Hence, the charge transport mechanism is non-resonant tunnelling[10–12]. A fair agreement between experimentally measured and theoretically calculated resistances can be obtained for molecular junctions with two chemisorbed thiol–gold contacts, taking into account that different contact geometries can lead to an order of magnitude difference in the computed results[13].

Progress in the study of discrete devices, not to mention their integration into circuits, is severely hampered by their limited reliability, stability and, especially, yield. Electrical shorts in the SAM are readily formed upon vapour deposition of the top electrode[14]. This has limited the diameter of the first reported molecular junctions to several tens of nanometres[15]. Recently, a statistical analysis has been reported for manually measured molecular junctions with diameter of 2 μm (ref. 16), which resulted in a yield of functional junctions of 1.2% (156 out of 13,440). The formation of shorts can be prevented by applying a conducting barrier layer between the SAM and the top electrode. A yield of unity has been reported for discrete large-area junctions by using the conducting polymer poly(3,4-ethylenedioxythiophene) stabilized with polystyrene sulphonic acid (PEDOT:PSS) as a barrier[17]. To prevent crosstalk, the discrete junctions were processed in vertical interconnect holes, lithographically defined in photoresist.

Integration of discrete molecular junctions, however, requires additional patterning of both the bottom and top electrode as well as a second layer of interconnects. A bottleneck is the limited processing window; the process temperature has to be limited to only 50 °C to prevent deterioration of the SAM. Here we present a default process flow chart for simultaneously processing over 20,000 molecular junctions on 150-mm substrates. Integration is demonstrated in strings where up to 200 junctions are connected in series. The layout allows semi-automatic measurements of electrical transport properties. The yield of unity for such a large number of identically processed junctions enables us to statistically analyse reliability and reproducibility. Furthermore, the statistics obtained by varying the processing parameters and measuring the influence on the junction resistance allows for the tentative interpretation that the electrical transport through these monolayer junctions is factorized.

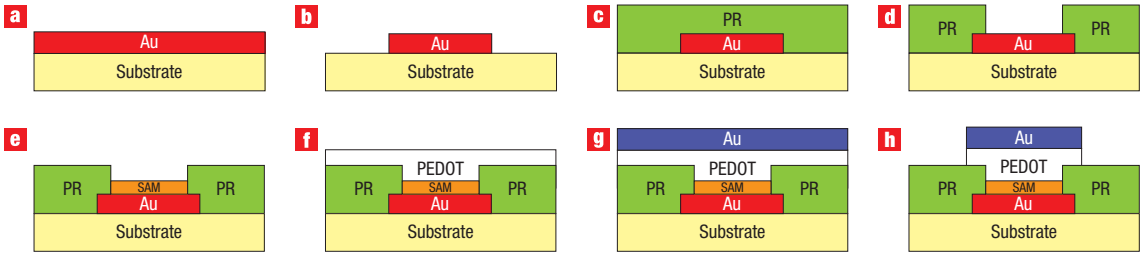

Figure 1 Schematic presentation of the process flow chart. a, Deposition of gold bottom electrode. **b**, Patterning the gold bottom electrode using photolithography. **c**, Spin-coating of negative photoresist (PR). **d**, Photolithographical definition of vertical interconnect. **e**, SAM formation. **f**, Spin-coating of PEDOT:PSS. **g**, Deposition of gold top electrode. **h**, Patterning of top electrode using photolithography.

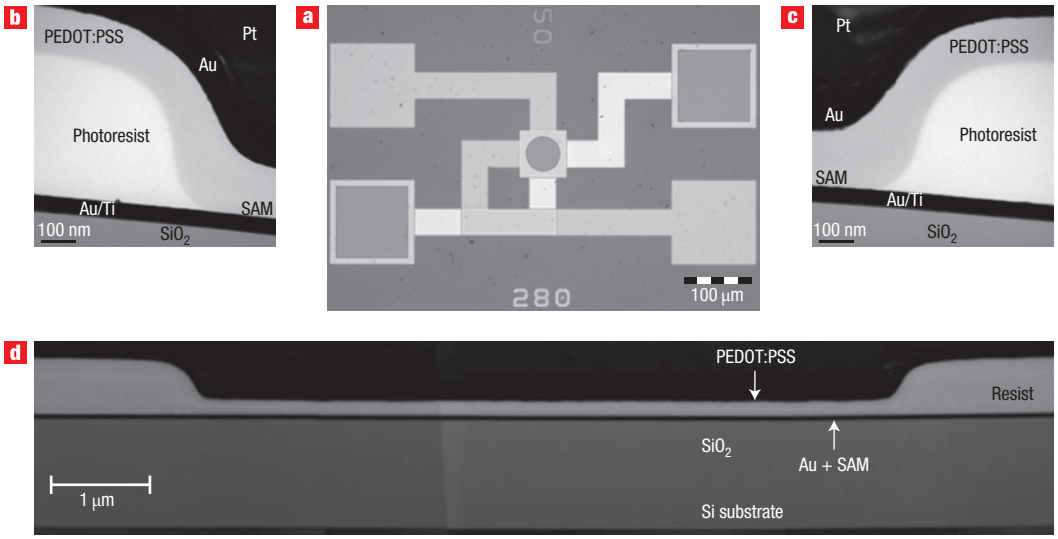

Figure 2 Cross-section of a molecular junction. a, Optical micrograph showing a circular molecular junction with a diameter of 50 μm, and the leads of a four-point Kelvin probe. **b**–**d**, Transmission electron spectroscopic images of a molecular junction of length 10 μm: the two ends of the junction in greater detail, clearly showing that the PEDOT:PSS layers follows the contours of the photoresist (**b**,**c**); conformal coverage of PEDOT:PSS in the via with a typical positive slope of 30° (**d**).

FABRICATION OF MOLECULAR JUNCTIONS

The process flow chart is schematically presented in Fig. 1. Note that the junction resistance and scaling with surface area depend on processing conditions such as the type of photoresist, chemical composition of the monolayer, the use of surfactants and the drying conditions of the PEDOT:PSS. A detailed overview of experimental methods, technological details, junction characterization and discussion thereof is presented in the Supplementary Information. This detailed information allows for easy reproduction of the junctions. Here we discuss the default process flow chart in which alkane(di)thiols are used to benchmark the resistances versus literature data.

A 150-mm c-silicon monitor wafer with a 1-μm thermally grown SiO_2 layer was used as substrate. A gold electrode was deposited and patterned by I-line projection photolithography to obtain the bottom contacts and the first layer of interconnects. Titanium was used as an adhesion layer. The root-mean-square roughness for a 50-nm-thick electrode was 0.7 nm. To electrically isolate the junctions, processing is performed in vertical interconnects (vias) defined in photoresist. As a default we used the epoxy-based negative photoresist L6000.5. The diameter of the circular vias ranged from 1 to 50 μm. After developing the photoresist and cleaning the gold, an alkanethiol monolayer was self-assembled from solution. The SAM coverage depended on temperature, concentration of the alkanethiol in solution and on the incubation time[18,19]. To obtain a densely packed SAM we used 1 mM solutions and an incubation time of three days. To avoid any oxidation, the self-assembly took place in an inert atmosphere. As an empirical quality check for SAM formation we used complete dewetting of the wafer by ethanol. The microstructure was investigated with AFM, XPS, Kelvin probe, ellipsometry and contact angle measurements (for results, see Supplementary Information, Table S2). The process technology yields densely packed SAMs (see Supplementary Information, Section 3).

On top of the SAM, a thin layer of PEDOT:PSS is spin-coated. The electrically conducting PEDOT:PSS layer prevents the formation of top-down shorts upon deposition of a gold top electrode. The difference in surface tension between the hydrophobic SAM and the waterborne PEDOT:PSS prevents them from mixing. We added 5% DMSO to PEDOT:PSS, yielding a conductivity of 300 S cm^{-1}. Homogeneous PEDOT:PSS films were obtained when, directly after spin–coating, the film

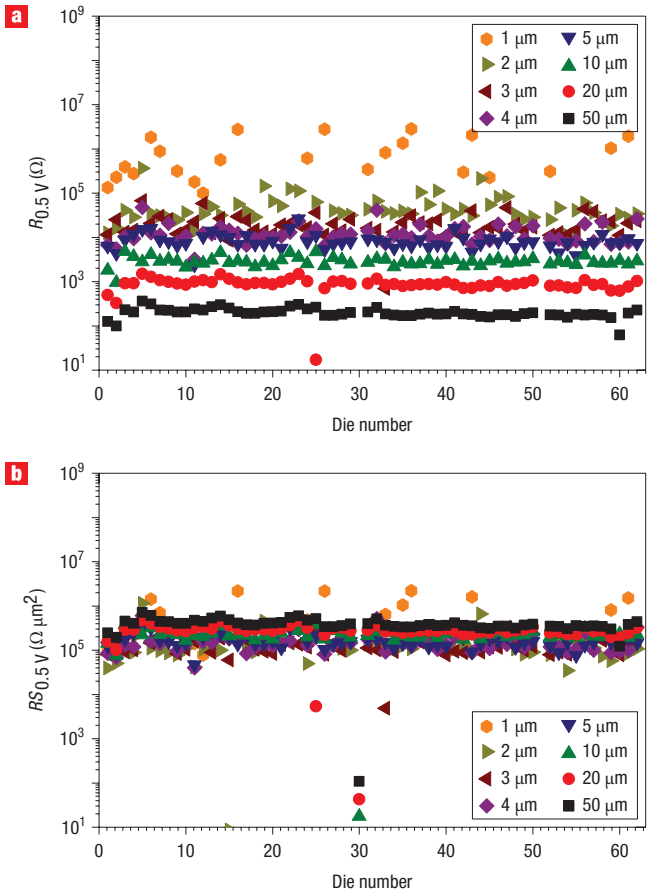

Figure 3 Statistical representation of junction resistances. a, Automatically measured resistances of $C_{18}H_{37}$-SH SAM junctions with diameter between 1 and 50 μm as a function of die number. **b**, The normalized resistance (in Ω μm²) as a function of die number.

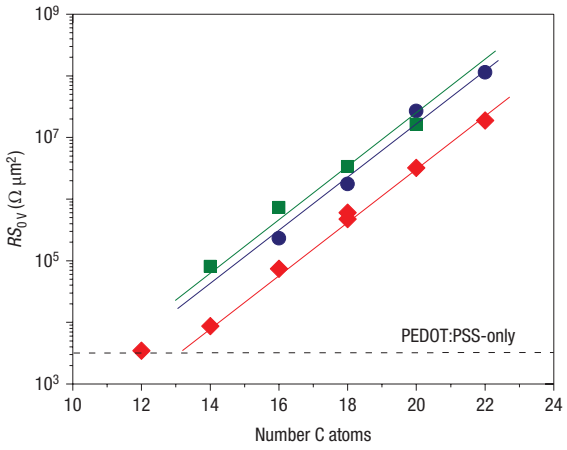

Figure 4 Resistance as a function of process parameters. The normalized resistance of alkane-monothiol C_nH_{2n+1}-SH SAM junctions with $n = 14–22$, averaged over all junctions on the wafer, on a semi-logarithmic scale as a function of the number of carbon atoms in the backbone. The dotted line represents the PEDOT:PSS-only value. The red diamonds represent devices made with the default process flowchart using L6000.5 photoresist and Agfa ICP new-type PEDOT:PSS with 5% DMSO. The blue circles represent the averaged normalized junction resistances using PH500 PEDOT:PSS with 5% DMSO. The green squares represent the averaged normalized resistances when MA1407 photoresist is used instead of L6000.5. The three solid lines represent a fit to the data points.

was dried on a hot plate at 100 °C. However, SAMs of alkanethiols on gold are unstable at elevated temperatures. To avoid any thermal deterioration of the SAM we limited the process window to 50 °C (see Supplementary Information, Fig. S3). Therefore, the PEDOT:PSS films were not dried at elevated temperatures but at room temperature in a dynamic vacuum of 1×10^{-3} mbar. Unfortunately, this drying procedure can lead to the formation of striations, that is, variations in radial thickness. Homogeneous PEDOT:PSS films could be made by careful adjustment of the processing conditions such as dispensing the solution over the whole 150-mm wafer and immediate drying the film after spin-coating.

The wetting of PEDOT:PSS on hydrophobic surfaces can be dramatically improved by adding surfactants. Using a non-ionic, fluorinated surfactant, uniform PEDOT:PSS films could be fabricated on SAMs with contact angles as large as 114°. The electrical resistance of the junction, however, is then comparable to that of PEDOT:PSS-only junctions, that is, junctions without a SAM.

The gold top contacts and the second layer of interconnects were defined in the top gold electrode by photolithography and dry etching. To stay within the thermal budget, the top gold electrode layer was not sputtered, but instead was evaporated. Finally, by reactive ion etching with the patterned top gold electrodes as a self-aligned mask, the redundant PEDOT:PSS outside the junctions was removed to prevent crosstalk.

An optical micrograph of a processed junction is presented in Fig. 2a. A cross-section of a molecular junction is obtained with focused ion beam milling. Transmission electron spectroscopic images are depicted in Fig. 2b–d. Both sides of the 10-μm junction are shown, and the chemical composition of the layers is indicated. From Fig. 2b–d the SAM layer itself cannot be resolved, but the conformal coverage of the PEDOT:PSS following the contours of the via is clearly observed, with the via having a typical positive slope of 30°.

ELECTRICAL CHARACTERIZATION OF JUNCTIONS AND STRINGS

Current density–voltage ($J–V$) characteristics have been measured for alkane-monothiol junctions C_nH_{2n+1}-SH with $n = 8–22$. The current densities for $n = 8$, 10 and 12 are indistinguishable from PEDOT:PSS-only junctions. Only for the longer alkane chains is the electrical transport unambiguously dominated by the SAM. The transport is symmetric and independent of temperature and at low bias the resistance is constant. With increasing bias the resistance decreases, resulting in nonlinear $J–V$ characteristics (see Supplementary Information, Fig. S8). Here we focus on the resistance at low bias. In Fig. 3a the junction resistances of $C_{18}H_{37}$-SH SAMs are presented as a function of diameter and die number. A wafer consists of 62 identical die structures. Each die contains via holes with diameters ranging from 1 to 50 μm, as indicated in the figure legend. The normalized resistances (in Ω μm²) are presented in Fig. 3b. Two dies (nos. 30 and 51) are shorted due to an artefact of the automatic prober and, therefore, are omitted. Figure 3 shows that the reproducibility is good, and that the yield is almost unity (see Supplementary Information, Fig S9). Furthermore, the resistance scales with area as expected for a parallel network of single-molecule junctions. Careful inspection of Fig. 3 reveals a slight increase in resistance with device area. (See Supplementary Information, Fig. S10, for a

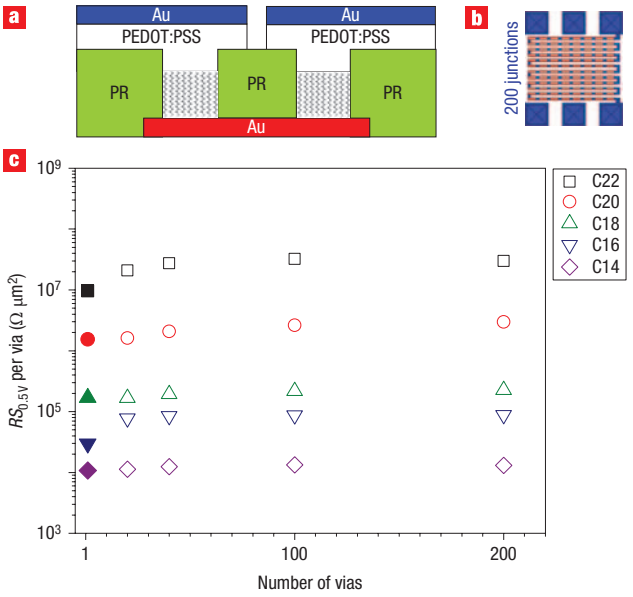

Figure 5 Integration of junctions in series. a, Schematic cross-section of a part of a string showing two connected junctions. **b**, Layout of strings in which a number of molecular junctions are connected in series. Each section contains two junctions. The red and blue colours represent the bottom and top gold layers, respectively. **c**, The normalized resistance of alkane-monothiol C_nH_{2n+1}-SH SAM junctions with $n = 14-22$, integrated in strings using the default process flow chart. The junctions are 5 μm in diameter. The normalized resistance per via is presented as function of the number of junctions. Values for discrete single junctions are included as filled symbols for comparison.

detailed analysis of scaling and a tentative interpretation based on PEDOT:PSS/SAM interaction that varies with surface area.)

If we define a junction as being electrically shorted when its resistance is equal to that of the PEDOT:PSS-only junction, then experimentally we find a yield of either about zero or unity. A yield of zero is obtained for fluorinated alkanethiols, and for alkane-monothiols onto which the PEDOT:PSS layer is processed with the use of a fluorinated surfactant. The reason for the low yield might be intermixing of SAM and PEDOT:PSS. Typically, however, the yield is about unity. Apparently, the technology is robust against imperfections in the SAM. We note that the bottom gold electrode is polycrystalline with a root-mean-square roughness of 0.7 nm, which is only slightly smaller than the length of the molecules, ~2–3 nm. The SAM is ordered but not single crystalline and, therefore, the monolayer contains a large number of structural defects distributed on a length scale smaller than the diameter of the junctions. The defects, however, do not lead to shorts, because the difference in surface tension between the SAM and PEDOT:PSS results in a poor wetting, which prevents intermixing. Consequently, PEDOT:PSS forms a badly adhering, but continuous film on top of the SAM.

The normalized resistance averaged over all junctions on the wafer is presented on a semi-logarithmic scale in Fig. 4 as a function of the number of carbon atoms in the alkanethiol backbone, n. The dotted line represents the PEDOT:PSS-only value. The resistance of the alkanethiol SAM junctions increases exponentially with the length according to $RS \approx \exp(\beta n)$. The decay constant β is calculated as 0.9 per carbon atom, which corresponds to 0.73 $Å^{-1}$. We investigated the influence of processing conditions on the junction resistance by varying the type of PEDOT:PSS and the type of photoresist. Default junctions were processed with L6000.5 as a photoresist and with PEDOT:PSS from Agfa (ICP new-type) that contains 5 vol % DMSO. Junctions were also made with PEDOT:PSS from H.C. Starck (viz. PH500). After adding 5% DMSO the bulk conductivity was comparable to that of Agfa, at ~300 S cm^{-1}. The yield of the junctions was again unity, but typically the wafers presented more inhomogeneities, like striations. The scaling of the resistance with surface area is less perfect and the standard deviations are slightly larger than with the default process flow chart. The averaged normalized resistances are presented in Fig. 4 as blue dots. The resistances are about a factor of 5 higher than those using the default process flow chart, but the exponential dependence on length and thus the decay constant is comparable. A similar behaviour is found when replacing the photoresist. Figure 4 shows the averaged normalized resistances when using MA1407 as photoresist instead of the standard L6000.5. The absolute values are larger than using the default process flow chart, but the exponential dependence and decay constant are comparable.

α,ω-Alkane-dithiols are used in MCBJs and C-AFM measurements to obtain strongly bound chemisorbed gold–sulphur contacts on both sides of the molecule. Because we use a physisorbed top contact consisting of PEDOT:PSS, replacing monothiols by dithiols is therefore not expected to improve the contact. Even though the use of dithiols might complicate the technology because α,ω-alkane-dithiols are more prone to oxidation and sensitive to moisture, we fabricated dithiol junctions using the default process flow chart. The normalized resistances are comparable to that of the monothiols (see Supplementary Information, Fig. S12). However, depending on the processing conditions the absolute values of the normalized resistance can easily be offset by a factor of a thousand.

The process technology developed comprises patterned interconnects in both top and bottom electrode layers. Therefore, strings can be fabricated in which a large number of molecular junctions are connected in series (Fig. 5a). The layout of strings as presented in Fig. 5b, shows that up to 100 sections, each containing two junctions, can be integrated. The normalized resistance per junction is given as a function of the number of junctions in Fig. 5c using the default process flow chart. The normalized resistance does not depend on the number of junctions, indicating a reproducible process technology with a yield of unity. The values from Fig. 4 for the discrete junctions are included for comparison as filled symbols and, typically, a fair agreement is obtained.

FACTORIZATION OF CHARGE TRANSPORT

The molecular junction presented here consists of a chemisorbed gold–sulphur bottom contact, an alkane backbone and a physisorbed SAM/PEDOT top contact. The junction thickness is smaller than the electron coherence length and, therefore, Ohm's law is not obeyed and the junction resistance cannot be obtained from a simple equivalent series circuit. The transport mechanism is non-resonant tunnelling and the transmission of a junction can be modelled with a multi-barrier tunnel model[20]. Here we take the resistance of a single molecule, R, at low bias according to ref. 21 as being factorized by

$$R = \frac{h}{2e^2} T^{-1} = 12.9\,\mathrm{k\Omega} T_{\mathrm{Au-S}}^{-1} T_{\mathrm{mol}}^{-1} T_{\mathrm{SAM\ PEDOT}}^{-1} \qquad (1)$$

where T is the overall transmission probability and where $T_{\mathrm{Au-S}}$, T_{mol} and $T_{\mathrm{SAM\ PEDOT}}$ are the transmission probabilities for the

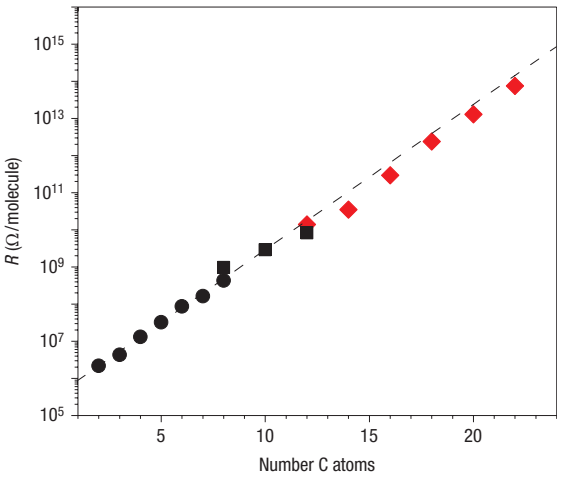

Figure 6 Summary of resistances. The resistance of alkane-monothiol C_nH_{2n+1}-SH SAM junctions with $n = 14-22$ calculated per molecule by taking a grafting density of 4.6×10^{14} cm^{-2} versus the number of carbon atoms in the backbone. Resistances were taken from Fig. 4 using the default process flowchart (red diamonds). Resistances of single molecule junctions obtained with MCBJ (filled circles) and C-AFM measurements (filled squares) on α,ω-alkane-diamines[2] and α,ω-alkane-dithiols[4] with two chemisorbed contacts are included for comparison. The dotted line is calculated using equation (2) with a decay coefficient β of 0.9 per carbon, using similar resistance contribution factors r_{Au-S} and $r_{SAM\ PEDOT}$. The electronic coupling strength that can be determined at the *y*-axis intercept differs by at most a factor of 10 for these sets of molecules.

gold–sulphur bottom contact, the molecule itself and the SAM/PEDOT top contact, respectively. Rewriting in practical terms yields

$$R = 12.9\,\mathrm{k\Omega}\; r_{Au-S} r_{mol} r_{SAM\ PEDOT} \qquad (2)$$

where r_{Au-S}, r_{mol} and $r_{SAM\ PEDOT}$ are unitless resistance contribution factors accounting for the resistance contribution of the bottom contact, the molecule and the top contact, respectively. The molecule contribution is given by $r_{mol} = \exp(\beta n)$, where β is the decay coefficient and n the number of carbon atoms in the backbone. The SAM junction resistance, assuming that cooperative effects can be disregarded[22], is given by the single-molecule resistance divided by the grafting density.

The factorization of the resistance explains both the length dependence and the offset due to processing. The bottom contact is a chemisorbed gold–sulphur bond that is the same for all junctions. When we vary the length of the molecule the resistance increases exponentially with the number of carbon atoms in the backbone by $R \approx r_{mol} = e^{\beta n}$. The value for the decay constant β is ~ 0.9 per carbon or 0.73 Å^{-1} assuming 1.22 Å for the length of a methylene group. When we keep the length of the molecule fixed and vary the processing of the top contact, then the resistance is proportional to the top contact resistance factor $r_{SAM\ PEDOT}$. Plotting the junction resistances on a semi-logarithmic scale as a function of the length of the molecule therefore yields parallel straight lines where the slope gives the decay coefficient β. The offset is determined by the technology through $r_{SAM\ PEDOT}$, which is a measure of the electronic coupling strength between the SAM and PEDOT:PSS. The sets of parallel straight lines are clearly observed in Fig. 4. We note that the interpretation is only phenomenological. A microscopic explanation for the dependence of the electronic coupling of the top contact on for instance the type PEDOT:PSS cannot be presented. There might be a relation with bulk conductivity, but that could not yet be demonstrated unambiguously.

To benchmark the data obtained, we present in Fig. 6 the resistance per molecule together with reported resistances from single-molecule junctions. The resistance per alkane-monothiol using the default process flow chart is calculated from Fig. 4 assuming a grafting density of 4.6×10^{14} cm^{-2}. As typical single-molecule resistances we took the values obtained from mechanically controlled MCBJs and C-AFM on α,ω-alkane-dithiols with two chemisorbed contacts[1–6]. Figure 6 shows a good agreement between the two datasets, with a single decay coefficient of 0.9 per carbon, a typical value for a saturated chain[23,24]. For the fit of Fig. 6 we used equation (2). We took r_{Au-S} to be similar to $r_{SAM\ PEDOT}$ and slightly lower than the published estimated value of 18.7 (ref. 21). This indicates that the SAM/PEDOT contact behaves electrically as a strongly bound contact. However, note that minor changes in the processing of PEDOT:PSS led to significant changes in the electronic coupling and hence to dramatic changes in the absolute value of the resistance. Therefore, a systematic variation of length of the molecule is required to separate its contribution to the transport from that of the processing.

In summary, we have presented a technology to fabricate and integrate molecular junctions on 150-mm wafers. The junction consists of a gold bottom electrode, a self-assembled alkanethiol monolayer, the conducting polymer PEDOT:PSS and a gold top electrode. On a single wafer more than 20,000 molecular junctions with diameter between 1 and 50 μm are fabricated simultaneously. Integration is demonstrated in strings where up to 200 junctions are connected in series. The yield is about unity. The junction resistances depend exponentially on the length of the alkane backbone. However, the absolute value of the resistance shows a technology-dependent prefactor: electrical transport through such junctions is factorized and the technology-dependent prefactor reflects the electrical coupling at the PEDOT:PSS and SAM contact. To understand the electrical transport through self-assembled monolayers, a systematic variation of the length of the molecule together with uniform processing of PEDOT:PSS over the whole wafer is required.

Received 20 May 2008; accepted 19 September 2008; published 19 October 2008.

References

1. Chen, F., Hihath, J., Huang, Z., Li, X. & Tao, N. J. Measurement of single-molecule conductance. *Annu. Rev. Phys. Chem.* **58,** 535–564 (2007).
2. Venkataraman, L. *et al.* Single-molecule circuits with well-defined molecular conductances. *Nano Lett.* **6,** 458–462 (2006).
3. Cui, X. D. *et al.* Reproducible measurement of single-molecule conductivity. *Science* **294,** 571–574 (2001).
4. Cui, X. D. *et al.* Changes in the electronic properties of a molecule when it is wired into a circuit. *J. Phys. Chem. B* **106,** 8609–8614 (2002).
5. Tao, N. J. Electron transport in molecular junctions. *Nature Nanotech.* **1,** 173–181 (2006).
6. Akkerman, H. B. & de Boer, B. Electrical conduction through single molecules and self-assembled monolayers. *J. Phys. Condens. Matter* **20,** 13001 (2008).
7. Porter, M. D., Bright, T. B., Allara, D. L. & Chidsey, C. E. D. Spontaneously organized molecular assemblies. 4. Structural characterization of n-alkyl thiol monolayers on gold by optical ellipsometry, infrared spectroscopy and electrochemistry. *J. Am. Chem. Soc.* **109,** 3559–3573 (1987).
8. Love, J. C., Estroff, L. A., Kriebel, J. K., Nuzzo, R. G. & Whitesides, G. M. Self-assembled monolayers of thiolates on metals as a form of nanotechnology. *Chem. Rev.* **105,** 1103–1169 (2005).
9. Vericat, C. *et al.* Surface characterization of sulfur and alkanethiol self-assembled monolayers on Au(111). *J. Phys. Condens. Matter* **18,** R867–R900 (2006).
10. Wang, W., Lee, T. & Reed, M. A. Electron tunnelling in self-assembled monolayers. *Rep. Prog. Phys.* **68,** 523–544 (2005).
11. Slowinski, K., Chamberlain, R. V., Miller, C. J. & Majda, M. Through-bond and chain-to-chain coupling. Two pathways in electron tunnelling through liquid alkanethiol monolayers on mercury electrodes. *J. Am. Chem. Soc.* **119,** 11910–11919 (1997).
12. Kim, Y.-H., Tahir-Kheli, J., Schultz, P. A. & Goddard III, W. A. First-principles approach to the charge-transport characteristics of monolayer molecular-electronics devices: Application to hexanedithiolate devices. *Phys. Rev. B* **73,** 235419 (2006).
13. Müller, K.-H., Effect of the atomic configuration of gold electrodes on the electrical conduction of alkanedithiol molecules. *Phys. Rev. B* **73,** 045403 (2006).

14. de Boer, B. *et al*. Metallic contact formation for molecular electronics: Interactions between vapour-deposited metals and self-assembled monolayers of conjugated mono- and dithiols. *Langmuir* **20,** 1539–1542 (2004).
15. Reed, M. A., Zhou, C., Muller, C. J., Burgin, T. P. & Tour, J. M. Conductance of a molecular junction. *Science* **278,** 252–254 (1997).
16. Kim, T. W., Wang, G., Lee, H. & Lee, T. Statistical analysis of electronic properties of alkanethiols in metal–molecule–metal junctions. *Nanotechnology* **18,** 315204 (2007).
17. Akkerman, H. B., Blom, P. W. M., de Leeuw, D. M. & de Boer, B. Towards molecular electronics with large-area molecular junctions. *Nature* **441,** 69–72 (2006).
18. Bain, C. D. *et al*. Formation of monolayer films by the spontaneous assembly of organic thiols from solution onto gold. *J. Am. Chem. Soc.* **111,** 321–335 (1989).
19. Akkerman, H. B. *et al*. Self-assembled-monolayer formation of long alkanedithiols in molecular junctions. *Small* **4,** 100–104 (2008).
20. Wang, G., Kim, T.-W., Lee, H. & Lee, T. Influence of metal–molecule contacts on decay coefficients and specific contact resistances in molecular junctions. *Phys. Rev. B* **76,** 205320 (2007).
21. Seminario, J. M. & Yan, L. Ab initio analysis of electron currents in thioalkanes. *Int. J. Quantum Chem.* **102,** 711–723 (2005).
22. Landau, A., Kronik, L. & Nitzan, A. Cooperative effects in molecular conduction. *J. Comp. Theor. Nanosci.* **5,** 535–544 (2008).
23. Tomfohr, J. K. & Sankey, O. F. Complex band structure, decay lengths and Fermi level alignment in simple molecular electronic systems. *Phys. Rev. B* **65,** 245105 (2002).
24. Tomfohr, J. K. & Sankey, O. F. Theoretical analysis of electron transport through organic molecules. *J. Chem. Phys.* **120,** 1542–1554 (2004).

Supplementary Information accompanies this paper at www.nature.com/naturenanotechnology.

Acknowledgements

We acknowledge financial support from the EU projects NAIMO (NMP4-CT-2004-500355). The work of E.C.P.S. forms part of the research program of the Dutch Polymer Institute (DPI) project no. 516. The work of H.B.A. and A.J.K. was financially supported by the Zernike Institute for Advanced Materials and NanoNed, a national nanotechnology program coordinated by the Dutch Ministry of Economic Affairs. The work in Mons is partly supported by the Interuniversity Attraction Pole IAP 6/27 Program of the Belgian Federal Government 'Functional supramolecular systems (FS2).' J.C. is a research fellow of FNRS. The work of S.P. and G.L. is supported by Fondazione Cariplo—Project TOLEDO. We acknowledge J.H.M. Snijders, C. van der Marel and H. Nulens for the XPS and AFM measurements, R.G.R. Weemaes for the FIB-TEM analysis, R. Schroeders for technical assistance, and N. Willard for fruitful discussions.

Author information

Reprints and permission information is available online at http://npg.nature.com/reprintsandpermissions/.
Correspondence and requests for materials should be addressed to D.M.D.L.